Cuadernos de Investigación Geográfica *Geographical Research Letters*	2017	Nº 43 (2)	pp. 697-718	ISSN 0211-6820 eISSN 1697-9540

DOI: http://doi.org/10.18172/cig.3235

TIMING AND EXTENT OF LATE PLEISTOCENE GLACIATION IN THE ARID CENTRAL ANDES OF ARGENTINA AND CHILE (22°-41°S)

J. ZECH[1*], C. TERRIZZANO[2], E. GARCÍA-MORABITO[2, 3], H. VEIT[2], R. ZECH[2]

[1]Max Planck Institute for the Science of Human History,
Kahlaische Strasse 10, 07745 Jena, Germany.
[2]Institute of Geography, University of Bern, Hallerstrasse 12, 3012 Bern, Switzerland.
[3] Instituto de Estudios Andinos "Don Pablo Groeber", Universidad de Buenos Aires - Conicet,
Buenos Aires, Argentina.

ABSTRACT. *The arid Central Andes are a key site to study changes in intensity and movement of the three main atmospheric circulation systems over South America: the South American Summer Monsoon (SASM), the Westerlies and the El Niño Southern Oscillation (ENSO). In this semi-arid to arid region glaciers are particularly sensitive to precipitation changes and thus the timing of past glaciation is strongly linked to changes in moisture supply. Surface exposure ages from study sites between 41° and 22°S suggest that glaciers advanced: i) prior to the global Last Glacial Maximum (gLGM) at ~40 ka in the mid (26°-30°S) and southern Central Andes (35°-41°S), ii) in phase with the gLGM in the northern and southern Central Andes and iii) during the late-glacial in the northern Central Andes. Deglaciation started synchronous with the global rise in atmospheric CO_2 concentration and increasing temperature starting at ~18 ka. The pre-gLGM glacial advances likely document enhanced precipitation related to the Southern Westerlies, which shifted further to the North at that time than previosuly assumed. During the gLGM glacial advances were favored by decreased temperatures in combination with increased humidity due to a southward shifted Intertropical Convergence Zone (ITCZ) and SASM. During the late-glacial a substantial increase in moisture can be explained by enhanced upper tropospheric easterlies as response to an intensified SASM and sustained La Niña-like conditions over the eastern equatorial Pacific that lead to glacial advances in the northern Central Andes and the lake level highstand Tauca (18-14 ka) on the Altiplano. In the southernmost Central Andes at 39º-41°S, further north at 31°S and in the northernmost Central Andes at 22°S glacial remnants even point to precipitation driven glaciations older than ~115 ka and 260 ka.*

Cronología y extensión de las glaciaciones pleistocenas tardías en los Andes Centrales áridos de Argentina y Chile (22°- 41°S)

RESUMEN. *Los Andes Centrales áridos constituyen un lugar clave para el estudio de los cambios en la dinámica e intensidad de los tres sistemas principales de circulación atmosférica presentes en Sudamérica: los vientos monzones, los vientos del oeste y el fenómeno El Niño-Oscilación del Sur. Debido a la aridez, los glaciares de esta región son particularmente sensibles a variaciones en las precipitaciones, por lo que la cronología de las glaciaciones está fuertemente controlada por el suministro de humedad. Las edades de exposición obtenidas en morrenas en un transecto comprendido entre 41° y 22° S de latitud indican avances glaciares que se sucedieron con anterioridad (unos 40 mil años BP) al Último Máximo Glaciar global (gLGM) para los Andes Centrales del sur (35°-41°S) y medios (26°-30°S). Avances en fase con el gLGM aparecen documentados en los Andes Centrales del sur y del norte, y durante el período Tardiglaciar en los Andes Centrales del norte. La deglaciación fue sincrónica a lo largo de todo el transecto y coincide con el incremento de los niveles de CO_2 globales. Los avances previos al gLGM documentan un posible aumento en las precipitaciones asociado a una migración hacia el norte de los vientos del oeste, de mayor magnitud a la asumida hasta el momento. Asimismo, durante el gLGM los avances glaciares fueron favorecidos por una disminución de la temperatura que coincide con un aumento de la humedad debido a la migración hacia el sur de la Zona de Convergencia Intertropical y de los vientos monzones. La mayor disponibilidad de humedad durante el período Tardiglaciar podría explicarse por un aumento de los vientos del este en las capas altas de la tropósfera, como respuesta a una intensificación de los vientos monzones y condiciones tipo La Niña sostenidas en el tiempo sobre la zona oriental del Pacífico ecuatorial. Estas condiciones condujeron a las glaciaciones registradas en los Andes Centrales del norte en concordancia con estadios de nivel alto en los lagos del Altiplano (fase Tauca, 18-14 mil años). Los restos de morrenas conservados en los extremos sur (39°-41°S) y norte (22°S) de los Andes Centrales, y a 31°S de latitud, indican a su vez avances glaciares anteriores a 115 y 260 ka, posiblemente controlados por las precipitaciones.*

Keywords: glacial chronology, arid Central Andes of Argentina and Chile, ^{10}Be surface exposure dating, paleoclimate reconstruction.

Palabras clave: cronología glaciar, Andes Centrales áridos de Argentina y Chile, Datación de exposición de superficies mediante ^{10}Be, reconstrucción paleoclimática.

Received: 7 February 2017
Accepted: 3 April 2017

*Corresponding author: Jana Zech, Max Planck Institute for the Science of Human History, Kahlaische Strasse 10, 07745 Jena, Germany. E-mail address: zech@shh.mpg.de

1. Introduction

The mass balance of glaciers is particularly sensitive to changes in temperature and precipitation. Thus, reconstructing past climate from paleoglaciers yields important insights into timing and magnitude of climate changes regionally and into changes in the atmospheric circulation system and related climate dynamics. The Argentinean and Chilean Central Andes (22°-41°S) situated between the tropical and extratropical atmospheric circulation systems are a key area to study past climate changes in the Southern Hemisphere on orbital and millennial timescale. Today the Central Andes are ice limited due to the low amount of precipitation (<400 mm, Bianchi and Yáñez, 1992; Haselton *et al*., 2002). However, pronounced geomorphological features like moraines record extensive glaciations in the past.

Establishing and correlating glacial chronologies along the arid Central Andes allows reconstructing primarily precipitation changes related to the dynamics of the three main atmospheric circulation systems over South America-the South American Summer Monsoon (SASM), the El Niño Southern Oscillation (ENSO) and the Westerlies. However, multiple questions remain regarding the influence and interplay between the tropical circulation system and the Westerlies in the core region of the arid Central Andes, the so-called Arid Diagonal (Fig. 1). In this review, we summarize previous research studies (Zech R. *et al*., 2007, 2008, 2009, 2010; Zech J. *et al*., 2009) about the late Pleistocene glaciation history and present new surface exposure ages (^{10}Be) along a N-S transect through the Central Argentinian and Chilean Andes between 41° and 22°S and interpret them in terms of climate variability.

2. Geographical Setting

The Andes are the dominant landform in South America (Fig. 1). The mountain chain is roughly 9000 km long and up to 750 km wide. Peaks can exceed altitudes of 6000 m. Ice caps and glaciers are present in the tropical and subtropical Andes north of 18°S and again south of 27°S.

Between ~ 18°S and 27°S, lies the so-called Arid Diagonal (Ammann *et al*., 2001). This core region of the Andes separates the regions to the north where moisture is primarily provided by the tropical circulation system from regions in the south where precipitation is provided by the Westerlies. No glaciers exist today in the Arid Diagonal due to extreme aridity (<100mm/a) even though peak altitudes lie above the zero-degree isotherm (Ammann *et al*., 2001; Zech R. *et al*., 2009).

The Central Andes extend along a transitional zone where precipitation has a distinct maximum (>80%) in the north (tropical and subtropical Andes), during austral summer associated with the South American Summer Monsoon (SASM) (Zhou and Lau, 1998; Garreaud *et al*., 2009) (Fig. 1). Between November and February, north-east trade winds transport moisture from the North Atlantic over the Amazon Basin. From there the South American Low Level Jet (SALLJ) flows southward along the Andean slope to the Gran Chaco basin. There the Chaco Low develops in the lower troposphere and the Bolivian High in the upper troposphere in response to strong insolation and convection. Ultimately, upper tropospheric easterlies, which intensify mutually with the Bolivian High, drag the

moisture from the lowlands into the Eastern Cordillera and onto the Altiplano (Garreaud *et al*., 2003; Vuille and Keimig, 2004). The intensity and location of this precipitation regime is modulated by the position of the Intertropical Convergence Zone (ITCZ), North Atlantic sea surface temperature (SST) and ENSO (Vuille *et al*., 2000; Garreaud and Aceituno, 2001; Vuille and Keimig, 2004). During La Niña years, SST in the eastern equatorial Pacific (EEP) cools. This strengthens the subsidence and enhances the upper tropospheric easterlies dragging more moisture into the Andean range. In contrast, during El Niño years the SST of the EEP rises and leads to convection, which weakens the upper tropospheric easterlies and causes anomalously dry conditions in the Andean range.

South of the Arid Diagonal (> 27°S) precipitation mainly falls during austral winter and is related to the Southern Westerlies, which provide moisture from the Pacific. The storm tracks shift from 55-45°S to their northernmost position at about 30°S and cause wet conditions in the Andean Cordillera (Garreaud *et al*., 2009). The Southern Westerlies also affect regions east of the Andean divide as far north as ~23-25°S when cold cut offs interact with warm and humid continental air, which generates large cloud cluster and

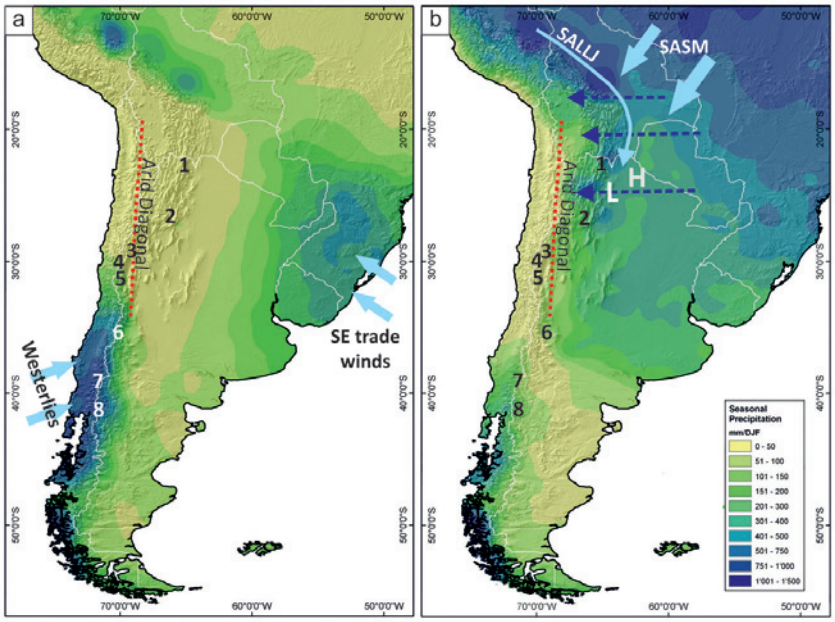

Figure 1. Location of research areas (numbers 1 to 8) and geographic setting in the Central Andes. a) mean austral winter precipitation regimen (June-July-August), b) mean austral summer precipitation regimen (DJF, December-January-February). Light blue arrows indicate the main atmospheric circulation systems, the South American Summer Monsoon (SASM) and the South American Low Level Jet (SALLJ) from the North and the Westerlies from the South. Dotted blue arrows show the upper tropospheric easterlies. Note the location of the Arid Diagonal in dotted red lines., L – Chaco Low, H – Bolivian High.

causes precipitation (Vuille and Ammann, 1997; Garreaud *et al*., 2009). Although the peak altitudes of the Andes drop from <6000 m north of 35ºS to only <3000 m further south, they remain glaciated, because precipitation increases to <2000 mm/a at 40°S (Garreaud and Aceituno, 2007) and temperatures decrease.

3. Material and Methods

3.1. Fieldwork

Fieldwork included geomorphological mapping of the research area as well as documentation (photography, geographical position using a handheld GPS, and shielding by surrounding topography). For surface exposure dating <0.5-1 kg of quartzite material was collected with hammer and chisel from sufficiently large and stable quartzite boulders from the stable top of the moraine ridges or glacio-morphological features with no signs of rock surface erosion in order to minimize the risk of too young exposure ages due to post-depositional processes, such as denudation, boulder exhumation, boulder toppling and rock surface erosion. When possible, we collected at least three samples on each moraine to identify outliers and avoid over or underestimations due to sample-specific effects (inheritance or post depositional instability). Details of field work and geomorphological mapping of the study sites can be found in the original publications (Zech R. *et al*., 2007, 2008, 2009, 2010; Zech J. *et al*., 2009).

3.2. ^{10}Be laboratory procedure and measurement

Physical and chemical pre-treatment of samples was conducted at the University of Bern following well established standard procedures involving: (i) sample crushing and sieving (to a size fraction of 250-400 μm), (ii) separating quartz from biotite and other magnetic minerals using a Frantz magnetic separator, (iii) three times rinsing of the sample with milliQ water as a first cleaning step, (iv) leaching of the sample with HCL (32%) to remove all organic remains, (v) leaching with HF (4%) four times to dissolve all minerals except of quartz and to remove atmospheric ^{10}Be from the mineral surface (vi) addition of a ^{9}Be carrier (~300 µg) followed by total dissolution in HF (40%), (vii) beryllium extraction through anion and cation exchange column chromatography, (viii) pH-sensitive precipitation and oxidation, and (ix) measuring the ^{10}Be/^{9}Be ratio at the ETH Zurich tandem AMS facility. Samples from Cordón de Doña Rosa, Bariloche, Cerro Fredes, El Encierro valley and Tres Lagunas were normalized to standard S555, with a nominal value of ^{10}Be/^{9}Be = 95.5 x 10^{-12} (± 2.5%). Samples from Las Leñas were normalized to standard S2007, with a nominal value of ^{10}Be/^{9}Be = 30.8 x 10^{-12} (± 2.5%, Kubik and Christl, 2010). Samples from Nevados de Chusca (Sierra de Quilmes) and the Rucachoroi valley were normalized using both standards depending on the sample (see Table 1).

3.3. Exposure age calculation and interpretation

Exposure ages were calculated or re-calculated from previous publications of Zech R. *et al*. (2007, 2008, 2009, 2010), Zech J. *et al*. (2009) with the CRONUS Calc v.2.0 (http://

Table 1. Compiled sample data. [a] Blank – corrected ^{10}Be concentrations. Standard S555 has a nominal value of $^{10}Be/^{9}Be = 95.5 \times 10^{-12}$ whereas standard S2007 has a nominal value of $^{10}Be/^{9}Be = 30.8 \times 10\text{-}12$. [b] ^{10}Be exposure ages calculated under the assumption of no erosion with the CRONUS Calc 10Be–26Al calculator, version 2.0 (Marrero et al., *2016), using a ^{10}Be half-life of 1.387 Ma and a rock density of 2.7 g/cm³. We applied the time and nuclide dependent scaling scheme of Lifton and Sato (SA, Lifton* et al., *2014). Topographic shielding was considered negligible, no corrections were applied.*

Sample I.D.	Latitude S (dd)	Longitude W (dd)	Altitude (m)	Thickness (cm)	^{10}Be concentration (at g^{-1}) [a]	Uncertainty in ^{10}Be concentration	^{10}Be Standardization	^{10}Be age (ka) [b]	±1σ (int)	±1σ (ext)
Rucachoroi Valley										
RU11	-39,1912	-71,3203	1800	3	292475,4704	19071,29298	S555	18,3	1,2	1,8
RU12	-39,1912	-71,3203	1801	3	270068,7001	7592,597697	S555	16,9	0,5	1,3
Ru21	-39,2118	-71,2953	1358	3	206286,96	10682,59484	S555	18,2	1,0	1,6
Ru31	-39,2516	-71,2217	1238	3	218207,2778	17453,39566	S555	20,8	1,6	2,2
Ru32	-39,2517	-71,2207	1241	3	178710,43	11699,341	S555	17,4	1,2	1,7
Ru51	-39,2529	-71,1846	1593	3	602373,4392	24608,72204	S555	40,9	1,6	3,3
Ru52	-39,2529	-71,1846	1594	3	504748,8124	23761,8293	S555	34,8	1,6	2,9
Ru53	-39,2527	-71,1843	1594	3	586595,8369	21816,48882	S555	39,9	1,5	3,1
RU61	-39,2011	-71,1072	1220	3	423317,406	24518,697	S555	39,1	2,3	3,6
RU62	-39,2011	-71,1072	1221	3	459499,466	30649,58608	S555	42	2,8	4,1
RC12	-39,2079	-71,2483	2026	3	271587,8449	16732,98535	S555	14,5	0,9	1,4
RC51	-39,2055	-71,1387	1303	3	524855,3905	32646,68034	S555	44,7	2,9	4,4
RC52	-39,2057	-71,1380	1297	3	455413,0931	25064,27513	S555	39,4	2,2	3,5
RC32	-39,2071	-71,2473	2018	3	282755,8412	12158,50117	S2007	15,1	0,7	1,3
RC42	-39,2201	-71,2235	1832	3	2010261,17	74379,66329	S2007	114,1	4,5	9,7
RU22	-39,2118	-71,2953	1358	3	284141,7263	13070,51941	S2007	24,4	1,1	2,1
Bariloche										
BA12	-41,0433	-71,1554	824	3	179766,7381	9,732240564	S555	22,9	0,0	1,7
BA15	-41,0436	-71,1543	834	3	252987,3419	6,08799911	S555	31,4	0,0	2,3
BA31	-40,9498	-71,0493	837	3	925240,7753	5,928614839	S555	113,6	0,0	8,7
BA32	-40,9498	-71,0500	841	3	811626,5457	4,37128927	S555	99,6	0,0	7,6
Las Leñas										
LL12	-35,1507	-70,0833	2322	3	403974,7478	17370,91415	S2007	20,1	0,8	1,5
LL13	-35,1519	-70,0899	2416	3	432903,0806	29004,5064	S2007	20,2	1,2	1,7
LL21	-35,1510	-70,0860	2347	3	379476,6701	30358,13361	S2007	18,8	1,4	1,9
LL22	-35,1504	-70,0838	2326	3	359522,4983	15818,98992	S2007	18,2	0,8	1,5

Sample I.D.	Latitude S (dd)	Longitude W (dd)	Altitude (m)	Thickness (cm)	^{10}Be concentration (at g^{-1}) [a]	Uncertainty in ^{10}Be concentration	^{10}Be Standardization	^{10}Be age (ka) [b]	±1σ (int)	±1σ (ext)
LL31	-35,1511	-70,0855	2346	1	1619986,235	95579,18784	S2007	70,7	4,8	7,5
LL42	-35,1418	-70,0751	2228	3	1039966,516	41598,66064	S2007	50	2,5	5
LL51	-35,1439	-70,0812	2266	5	423251,4482	18199,81227	S2007	21,9	0,9	1,8
LL55	-35,1439	-70,0812	2266	5	526531,3978	23167,3815	S2007	26,6	1,1	2,2
El Encierro Valley										
EE11	-29,1300	-69,9000	3971	3	801054	4,21	S555	18,2	0,0	1,3
EE12	-29,1300	-69,9000	3971	3	783229	3,79	S555	17,9	0,0	1,3
EE22	-29,1300	-69,9000	3998	3	732037	3,76	S555	16,5	0,0	1,3
EE24	-29,1300	-69,9000	3994	3	764244	4,22	S555	17,2	0,0	1,2
EE33	-29,1100	-69,9000	4055	3	791946	6,02	S555	17,3	0,0	1,3
EE34	-29,1100	-69,9000	4029	3	1004234	4,91	S555	21,2	0,0	1,3
EE42	-29,1000	-69,9000	3955	3	838268	4,29	S555	19,1	0,0	1,2
EE51	-29,0900	-69,9000	3900	3	897528	4,29	S555	20,6	0,0	1,2
EE62	-29,0700	-69,9000	3688	3	755000	5,30	S555	19,8	0,0	1,1
EE63	-29,0700	-69,9000	3684	3	530162	4,26	S555	14,3	0,0	1,1
EE71	-29,0700	-69,9000	3678	3	1472753	4,15	S555	34,9	0,0	2,1
Cordón Doña Rosa										
DR11	-30,6779	-70,3749	3806	3	765651,2577	29460,21785	S555	18,1	0,7	1,5
DR13	-30,6761	-70,3715	3762	3	824157,947	31862,85855	S555	19,6	0,6	1,3
DR21	-30,6792	-70,3682	3734	3	1128268,419	44027,71889	S555	26	1,0	2
DR31	-30,6813	-70,3648	3686	3	716976,0649	28972,33174	S555	18,1	0,7	1,5
DR32	-30,6819	-70,3645	3683	3	905738,2906	33326,59704	S555	21,8	0,8	1,6
DR33	-30,6823	-70,3643	3683	3	806142,3623	25377,00632	S555	19,9	0,5	1,2
DR41	-30,6890	-70,3602	3614	3	689475,5202	36650,717	S555	18,1	1,0	1,6
DR42	-30,6895	-70,3599	3603	3	727887,2134	30287,64895	S555	19,1	0,7	1,4
DR43	-30,6906	-70,3587	3591	3	701894,0233	27235,0654	S555	18,6	0,7	1,4
DR51	-30,7147	-70,3619	3383	3	5826265,15	174950,6708	S555	153	5,8	15
DR52	-30,7152	-70,3621	3376	3	1799290,427	54170,57292	S555	45,4	1,5	3,7
DR61	-30,7187	-70,3625	3316	3	1880550,585	67554,36275	S555	49,8	2,4	5,2
DR62	-30,7187	-70,3625	3317	3	1668547,082	55425,79478	S555	43,8	1,4	3,3
DR71	-30,7234	-70,3660	3293	3	1566903,121	87251,41434	S555	42,1	2,1	3,4
DR72	-30,7234	-70,3660	3294	3	755392,6705	31561,90845	S555	22,7	1,0	1,9

Sample I.D.	Latitude S (dd)	Longitude W (dd)	Altitude (m)	Thickness (cm)	^{10}Be concentration (at g^{-1}) [a]	Uncertainty in ^{10}Be concentration	^{10}Be Standardization	^{10}Be age (ka) [b]	±1σ (int)	±1σ (ext)
DR73	-30,7255	-70,3659	3300	3	1285536,277	53312,47271	S555	35,8	1,3	2,6
DR81	-30,7454	-70,4377	2536	3	1004253,102	42960,58525	S555	43,5	1,8	3,4
DR82	-30,7454	-70,4377	2537	3	1454161,104	61895,92367	S555	64,3	2,8	5,4
DR91	-30,7340	-70,5103	2058	3	592011,9591	26194,9345	S555	37	1,5	2,8
DR92	-30,7340	-70,5103	2059	3	578070,9778	18867,59095	S555	36,2	1,1	2,6
DR101	-30,7329	-70,5546	1772	3	279060,4521	29407,93011	S555	23	2,5	3
DR102	-30,7329	-70,5546	1773	3	417665,831	18187,13285	S555	32,8	1,4	2,6
Cerro Fredes										
CF21	-31,3898	-70,8291	3375	3	6768833,854	3	S555	176	0,0	14
CF23	-31,3888	-70,8291	3390	3	5321955,892	5,281098371	S555	132	0,0	11
CF31	-31,3933	-70,8298	3336	3	6657958,868	5,462600113	S555	178	0,0	14
CF33	-31,3933	-70,8298	3336	3	6386156,439	6,280127387	S555	170	0,0	16
CF41	-31,3970	-70,8383	3282	3	9306732,195	5,015974482	S555	257	0,0	22
Sierra de Quilmes										
CP11	-26,1614	-66,1709	4445	3	847922,056	44939,86897	S2007	16,3	0,9	1,6
CP14	-26,1666	-66,1728	4380	3	856816,8203	34272,67281	S2007	17	0,7	1,5
CP21	-26,1702	-66,1687	4274	3	848988,9212	40751,46822	S2007	17,7	0,9	1,6
CP22	-26,1703	-66,1692	4261	3	1685500,958	50565,02873	S2007	31,9	0,9	2,4
CP31	-26,1714	-66,1667	4273,5	3	1756462,201	52693,86604	S555	32,9	0,9	2,4
CP41	-26,1683	-66,1713	4297	3	1694468,67	105057,0575	S2007	31,5	1,9	2,9
NC11	-26,1669	-66,1792	4394	3	2361635,178	82657,23122	S2007	39,5	1,1	2,6
NC13	-26,1677	-66,1757	4378	3	2706698,759	81200,96276	S555	44,1	1,3	3,2
NC23	-26,1744	-66,1778	4301,5	3	855701,4535	35083,75959	S555	17,6	0,8	1,5
NC31	-26,1843	-66,1807	4174	3	718062,8088	21541,88427	S555	15,9	0,5	1,3
NC32	-26,1849	-66,1807	4158	3	673579,4402	32331,81313	S2007	15	0,7	1,3
Tres Lagunas										
LG11	-22,2006	-65,1231	4454	3	907224,78804	36288,99	S555	18,9	0,7	1,4
LG15	-22,2008	-65,1211	4469	3	801528,48509	39274,90	S555	16,7	0,9	1,5
LG21	-22,2036	-65,1200	4485	3	1077463,946	59260,52	S555	21,2	1,0	1,6
LG22	-22,2025	-65,1147	4509	3	1148846,38899	58591,17	S555	22,1	1,1	1,9
LG23	-22,2028	-65,1153	4506	3	5984211,01663	179526,33	S555	104,2	2,7	7,1
LG25	-22,2037	-65,1209	4478	3	766881,0404	29908,36	S555	16	0,7	1,4

Sample I.D.	Latitude S (dd)	Longitude W (dd)	Altitude (m)	Thickness (cm)	^{10}Be concentration (at g^{-1}) [a]	Uncertainty in ^{10}Be concentration	^{10}Be Standardization	^{10}Be age (ka) [b]	±1σ (int)	±1σ (ext)
LG31	-22,1861	-65,1036	4480	3	788408,62047	40208,84	S555	16,4	0,9	1,5
LG33	-22,1844	-65,1022	4471	3	869186,22613	45197,68	S555	18	0,9	1,6
LG41	-22,1875	-65,1017	4454	3	725601,48525	28298,46	S555	15,3	0,6	1,2
LG42	-22,1874	-65,1014	4455	3	735323,86818	57355,26	S555	15,5	1,2	1,7
LG51	-22,2019	-65,1217	4453	3	898603,72406	42234,38	S555	18,7	0,8	1,5
LG52	-22,2019	-65,1221	4444	3	828984,07154	29843,43	S555	17,5	0,6	1,4
LG53	-22,2016	-65,1234	4437	3	4781685,60940	262992,71	S555	87,6	5,8	9,6
LG61	-22,1916	-65,1336	4300	3	4145938,81425	228026,63	S555	80,6	5,8	9,5
LG62	-22,1924	-65,1331	4316	3	8956256,048	268687,68	S555	176	5,9	16
LG63	-22,1929	-65,1331	4320	3	6197618,052	185928,54	S555	116,8	3,6	9,1
LG64	-22,1936	-65,1331	4329	3	4130230,64588	128037,15	S555	78,8	3,3	7,9
LG65	-22,1944	-65,1325	4331	3	8832818,83	468139,40	S555	170	11,6	20
LG72	-22,1916	-65,1202	4379	1	601665,8151	20456,64	S555	13	0,5	1,2
LG73	-22,1919	-65,1203	4375	1	651684,6613	25415,70	S555	14,2	0,6	1,2
LG76	-22,1949	-65,1217	4377	1	867903,5599	34716,14	S555	18,5	0,7	1,5
LG81	-22,2000	-65,1198	4425	4	797787,2498	31113,70	S555	17,1	0,7	1,4
LG83	-22,1998	-65,1427	4421	4	727854,4987	29114,18	S555	15,7	0,7	1,4
LG92	-22,2055	-65,1097	4573	1	647557,8311	28492,54	S555	12,7	0,7	1,2
LG93	-22,2055	-65,1109	4561	2	697817,0315	30006,13	S555	14	0,6	1,2
LG95	-22,2038	-65,1106	4563	5	3315979,464	149219,08	S555	56,2	30,4	5,8
TL11	-22,2053	-65,1274	4403	2	814784,0587	26073,09	S555	17,4	0,6	1,4
TL12	-22,2038	-65,1274	4407	5	941697,5045	38609,60	S555	20	0,6	1,3
TL21	-22,2049	-65,1298	4411	2	1476690,154	48730,78	S555	28,6	0,9	2,1
TL22	-22,2049	-65,1298	4414	2	1021134,781	43908,80	S555	20,8	0,7	1,4
PN11	-22,2174	-65,1413	4340	3	1201917,269	42067,10	S555	24,9	0,8	1,8
PN12	-22,2258	-65,1381	4372	3	1711091,64648	70154,76	S555	33,2	1,2	2,5
PN21	-22,2261	-65,1393	4442	3	986992,10861	41453,67	S555	20,2	0,7	1,3
PN23	-22,2250	-65,1372	4387	3	848202,21404	64463,37	S555	18,3	1,3	1,9
PN22	-22,2260	-65,1404	4366	3	777149,66766	36526,03	S555	17	0,8	1,5

[a] Blank-corrected ^{10}Be concentrations. Standard S555 has a nominal value of ^{10}Be/^{9}Be =95.5 x 10-^{12} whereas standard S2007 has a nominal value of ^{10}Be/^{9}Be =30.8 x 10^{-12}

[b] ^{10}Be exposure ages calculated under the assumption of no erosion with the CRONUS Calc ^{10}Be–^{26}Al calculator, version 2.0 (Marrero *et al*. 2016), using a ^{10}Be half-life of 1.387 Ma and a rock density of 2.7 g/cm^{3}. We applied the time and nuclide dependent scaling scheme of Lifton and Sato (SA, Lifton *et al*. 2014). Topographic shielding was considered negligible, no corrections were applied.

web1.ittc.ku.edu:8888/2.0/html/al-be/), described by Marrero *et al*. (2016), applying the nuclide and time dependent scaling model of Lifton and Sato (SA or LSD, Lifton *et al*., 2014) with a production rate of 3.92 ± 0.31 atoms g^{-1} yr^{-1} (Phillips *et al*., 2016). We preferred to use this scaling model because it includes an updated geomagnetic and solar modulation framework, accounting for the effect of these factors on the cosmic-ray spectra. It also includes altitudinal scaling for separate nuclides (Lifton *et al*., 2014). CRONUS Calc uses a ^{10}Be half-life of ~1.39 Ma (Chmeleff *et al*., 2010; Korschinek *et al*., 2010).

Exposure ages were corrected for sample thickness. Topographic shielding was considered negligible and no corrections were applied (Table 1). We excluded shielding effects of vegetation and snow cover and considered negligible erosion as well as persistent arid conditions in the investigated areas of this review since the early Holocene result in minimal soil development and a scarce vegetation cover, so that obtained surface exposure ages represent minimum ages.

In principle, it is possible to find boulders with inherited cosmogenic ^{10}Be from a previous exposure history in a moraine ridge, which would provide an older than expected surface exposure age. However, the probability is assumed to be very low (<3%) (Putkonen and Swanson, 2003; Heyman *et al*., 2011). Moraine boulders can experience post-depositional processes (e.g. denudation, boulder exhumation, boulder toppling and rock surface erosion) resulting in too young exposure ages as well. Except in cases where there are clear statistical or stratigraphical outliers, we followed the approach of the 'oldest age model' (Briner *et al*., 2005; Zech R. *et al*., 2005), according to which the oldest boulder is a minimum estimate for the moraine age and beginning of ice retreat. Sample details and surface exposure ages are compiled in Table 1.

4. Glacial chronology

4.1. South of the Arid Diagonal (41°-29°S)

4.1.1. Rucachoroi valley (~39°S) and Bariloche (41°S)

In the Rucachoroi valley the maximum ice extent for the most extensive glacial advance is marked by the outermost moraine, which yielded a minimum exposure age of 44.7 ± 4.4 ka (Fig. 2). Further up valley an end moraine marks the position of the glacial front during the gLGM (~26 ka, Peltier and Fairbanks, 2006; Clark *et al*., 2009), dated to 20.8 ± 2.2 ka. Deglaciation of the valley started at about 18 ka, according to the minimum exposure age of 18.3 ± 1.8 (sample RU 11, Table 1, Fig. 2). However, note that on the cirque north of the main valley a minor late glacial advance is dated to 15.1 ± 1.3 ka which is in phase with the Tauca lake transgression phase on the Altiplano (18-14 ka, Placzek *et al*., 2011) and Heinrich I (Heinrich, 1988; Hemming, 2004). Also, a sample dated to 114.1 ± 9.7 ka may be documenting the oldest advance in this valley. Near Bariloche, at the confluence of the Nahuel Huapi glacial lake and the Limay river (Fig. 3), four exposure ages of two moraine remnants tentatively document glacial advances at 113.6 ± 8.7 ka and 31.4 ± 2.3 ka, clearly predating the gLGM.

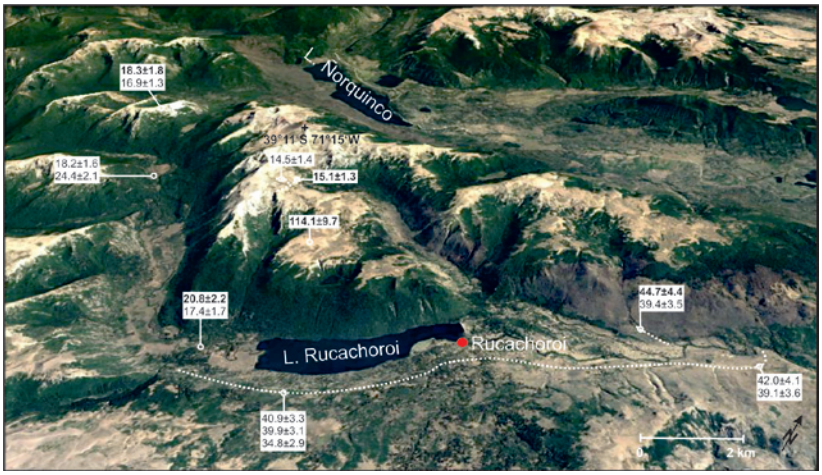

Figure 2. Google earth image of the Rucachoroi valley with the homonymous locality and lake. Circles indicate the sampling sites, White dashed lines show the crest of the frontal and lateral moraines of the local last glacial maximum advance in the valley. Bold ages show the interpreted deposition age. Shown ^{10}Be surface exposure ages were re-calculated from Zech et al. *(2008) applying the scaling system of Lifton and Sato (SA, Lifton* et al.*, 2014).*

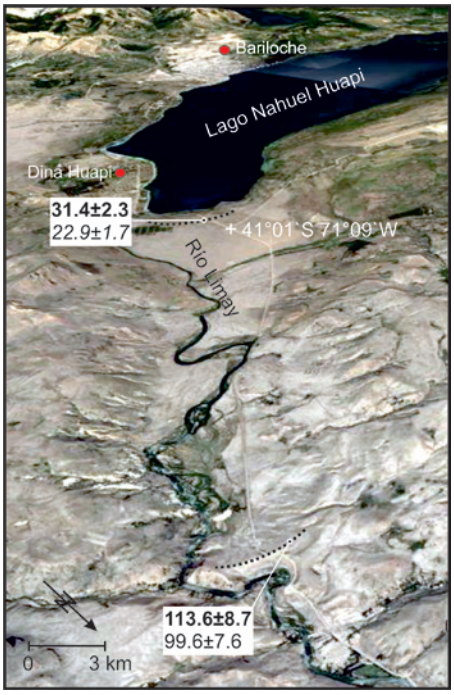

Figure 3. Google earth image of our study area near Bariloche. Black dashed lines: sampled frontal moraines. Bold ages show the interpreted deposition age. ^{10}Be surface exposure ages are calculated applying the scaling system of Lifton and Sato (SA, Lifton et al.*, 2014).*

4.1.2. Las Leñas (35°S)

At Las Leñas glaciers reached their maximum position most likely around 50.0 ± 5.0 ka (Fig. 4). Although this age has to be interpreted carefully, it documents the maximum ice extent for the most extensive glacial advance. Prominent, sharp crested lateral moraines document the most extensive advance during the gLGM at 21.9 ± 1.8 ka. Glacier climate modelling results for those moraines (Wäger, 2009) suggest that enhanced precipitation in combination with a temperature reduction of -5 to -8°C caused this gLGM advance. Deglaciation started at around 18.8 ± 1.9 ka.

Figure 4. Google earth image of Las Leñas. Black dashed lines: sampled moraines. Bold ages show the interpreted deposition age. [10]Be surface exposure ages are calculated applying the scaling system of Lifton and Sato (SA, Lifton et al.*, 2014).*

4.1.3. El Encierro valley (29°S), Cordón de Doña Rosa (30°S) and Cerro Fredes (~31°S)

In El Encierro valley a well-preserved end moraine marks the maximum ice extent for the most extensive glacial advance dated to 34.9 ± 2.1 ka (Fig. 5). During the gLGM the valley was still covered by a glacier that reached its maximum extent before 21.2 ± 1.3 ka. Deglaciation started shortly after at around 18 ka. Numerical modelling results from a glacier-climate study (Kull *et al*., 2002) indicate a temperature depression of 5.5°C and a precipitation increase to 550 mm/a for the gLGM glacial advance. This suggests that increased humidity coupled to the temperature minima during the gLGM played an important role for the glacial advances in the southern and northern part of the Arid Diagonal.

In the Cordón de Doña Rosa (30°S, Fig. 6) the maximum ice extent for the most extensive glacial advance is marked by a lateral moraine yielding a minimum ^{10}Be surface exposure age of 49.8 ± 5.2 ka in the main valley. In the adjacent valleys to the north the maximum ice extent is marked by lateral moraines yielding ^{10}Be surface exposure ages of 37.0 ± 2.8 ka and 32.8 ± 2.6 ka. Due to the smaller catchment size we conclude that glaciers in the adjacent valleys most likely prevailed some ~10 ka longer then in the main valley. Only in the catchment of the main valley a gLGM glacial advance is dated to 21.8 ± 1.6 ka.

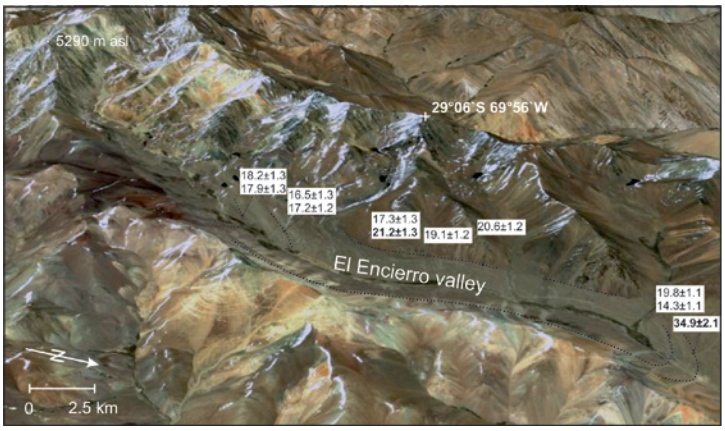

Figure 5. Google earth image of the El Encierro valley. Black dashed lines: sampled moraines. Bold ages show the interpreted deposition age. [10]Be surface exposure ages are re-calculated from Zech et al. *(2008) applying the scaling system of Lifton and Sato (SA, Lifton* et al.*, 2014).*

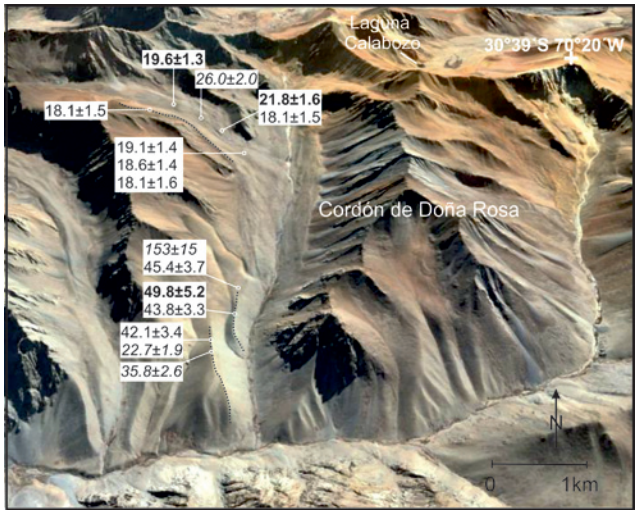

Figure 6. Google earth image of Cordón de Doña Rosa, Black dashed lines: main moraines, white circles indicate the collected samples and their obtained ages. [10]Be surface exposure ages are re-calculated from Zech et al. *(2008) applying the scaling system of Lifton and Sato (SA, Lifton* et al.*, 2014).*

Deglaciation started around 19.6 ± 1.3 ka in agreement with the global atmospheric CO_2 rise. We consider the exposure age of 153 ± 15 ka as too old due to pre-exposure.

At Cerro Fredes (31°S) the maximum ice extent for the most extensive glacial advance is documented by well-preserved moraines with ^{10}Be surface exposure ages of 257.0 ± 22 ka and 178.0 ± 14 ka (Fig. 7). Together with ages reported by Terrizzano *et al*. (2016) at 32°S on the Argentinian slope, these ages are so far the oldest evidence for a glaciation in the Central Andes dated with ^{10}Be SED.

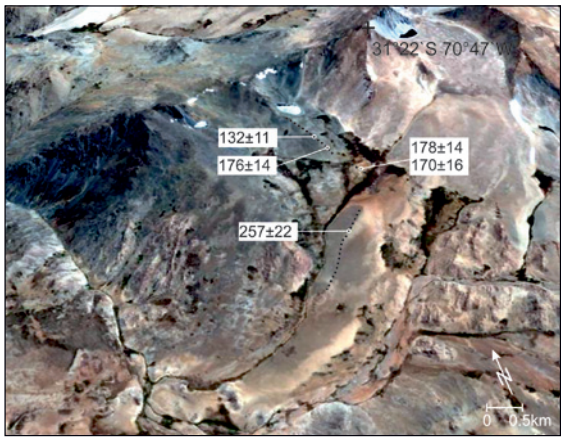

Figure 7. Google earth image of Cerro Fredes. Black dashed lines: sampled moraines. [10]Be surface exposure ages are calculated applying the scaling system of Lifton and Sato (SA, Lifton et al.*, 2014).*

4.2. At the latitude of the Arid Diagonal (26°-22°S)

4.2.1. Sierra de Quilmes (~26°S)

The Sierra de Quilmes (~26°S) is situated in the centre of the Arid Diagonal. Here, at the essentially distal end of the influence region of the SASM and the Southern Westerlies, precipitation is less than 400 mm/a (Bianchi and Yáñez, 1992; Haselton *et al*., 2002) on the eastern side of the Andes and less than 100 mm/a on the western side. An important increase in precipitation is thus necessary to provide glacial advances. However, well preserved glacial troughs from peaks of Cerro Pabellón (~5000 m a.s.l.) and Nevados de Chusca (~5400 m a.s.l.) reach down to ~3800 m a.s.l. documenting massive glaciations in the past (Fig. 8). The most extensive glaciation in the Nevados de Chusca Valley is

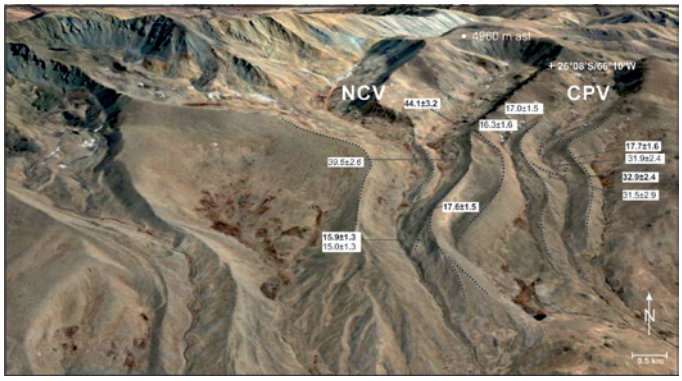

Figure 8. Google earth image of Sierra de Quilmes. Black dashed lines: sampled moraines. NCV: Nevados de Chusca Valley, CPV: Cerro Pabellón Valley. Bold ages show the interpreted deposition age. [10]Be surface exposure ages are calculated applying the scaling system of Lifton and Sato (SA, Lifton et al.*, 2014).*

documented by a well-preserved moraine dating to 44.1 ± 3.2 ka. Although the lower parts of the pronounced lateral moraines in the Nevados de Chusca Valley have not been sampled and dated, we can infer from the stratigraphic situation, that they must have been deposited between 44.1 ± 3.2 ka and 17.6 ± 1.5 ka. Deglaciation started at 17.6 ± 1.5 ka in phase with the global atmospheric CO_2 rise after 18 ka interrupted only by a minor re-advance at around 15.9 ± 1.3 ka synchronous with the lake transgression phase Tauca (Placzek *et al*., 2011). In the Cerro Pabellón Valley the maximum ice extent is dated to 32.9 ± 2.4 ka. Deglaciation started around 17.7 ± 1.6 ka. Catchment size (Nevados de Chusca Valley: ~21 km^2 vs. Cerro Pabellón Valley: ~3.6 km^2) and altitude differences (Nevados de Chusca Valley: ~5400m a.s.l. vs. Cerro Pabellón Valley: ~5000 m a.s.l.) between both valleys can help to explain the different preservation of the maximum ice extent predating the gLGM and the late-glacial glacial advances.

4.2.2. Tres Lagunas (~22°S)

The Tres Lagunas site and the adjacent valley of Peña Negra (Fig. 9) are located in the Sierra de Santa Victoria in NW Argentina, which forms the boundary between the eastern slope of the Andes to the east and the Altiplano/Puna plateau (~3500 m a.s.l.)

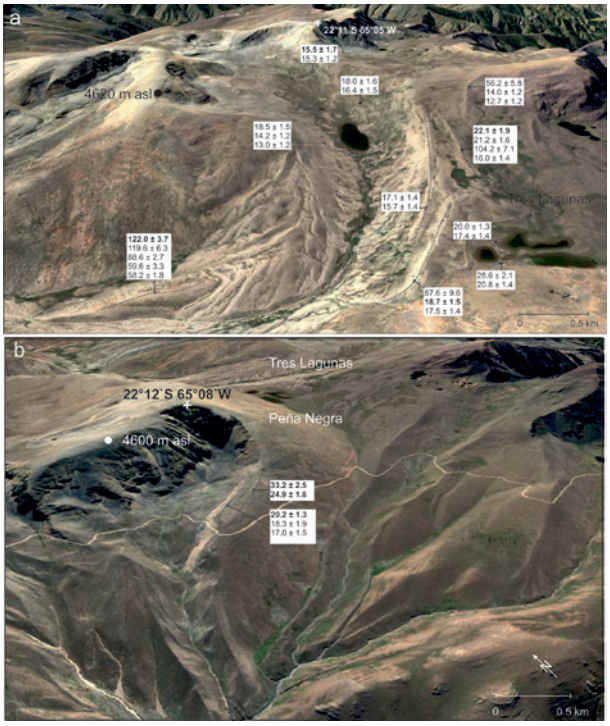

Figure 9. Google earth image of Tres Lagunas (a) and Peña Negra (b). Black dashed lines: sampled moraines. Bold ages show the interpreted deposition age. [10]Be surface exposure ages are re-calculated from Zech et al. *(2009a) applying the scaling system of Lifton and Sato (SA, Lifton* et al., *2014).*

to the west. The oldest and most extensive glaciation occurred around 122.0 ± 3.7 ka and coincides most likely with the Ouki lake transgression phase (120-95 ka) on the Altiplano (Placzek *et al*., 2011). A second distinct glaciation occurred at 22.1 ± 1.9 ka in phase with the lake transgression phase Sajsi (24-20 ka, Placzek *et al*., 2011) and the temperature minimum during the gLGM. Deglaciation started at around 18.7 ± 1.5 ka in phase with the global rise in atmospheric CO_2. High up in the catchment of Tres Lagunas site (~4500 m a.s.l.), a small glacial readvance is dated to 15.5 ± 1.7 ka in phase with the Tauca lake transgression phase on the Altiplano (Placzek *et al*., 2011). At Peña Negra the maximum ice extent is documented by a sharp crested lateral moraine dating to 24.9 ± 1.8 ka and 33.2 ± 2.5 ka. We tentatively suggest that this moraine correlates with the lateral moraines deposited during the gLGM at Tres Lagunas site. The inner lateral moraine was deposited at around 20.2 ± 1.3 ka. The steeper valley morphology of the Peña Negra Valley might explain the observed minor age differences.

5. Discussion

Studies on the timing of glaciation (Zech R. *et al*., 2008; Blard *et al*., 2009; Rodbell *et al*., 2009; Zech J. *et al*. 2009; May *et al*., 2011) and glacier-mass balance modelling (Kull *et al*., 2008; Blard *et al*., 2009) highlight the importance of precipitation for glacial advances in the semi-arid Central Andes. The oldest glacial advances, dated to ~115 ka and ~260 ka, are recorded south of and in the Arid Diagonal. The lack of information about wet or dry climate phases so far back in time prevents us to make further interpretations in terms of climate variability, although such ages may point to precipitation driven glaciations during Marine Isotope Stages (MIS) 8, 6 and in phase with the Ouki wet phase during MIS 5.

Glacial features from 41°S (Bariloche) to the north in the Ruchachoroi valley, Cordón de Doña Rosa, El Encierro valley, and even as far north as 26°S (Sierra de Quilmes) document that maximum ice extent for the most extensive glacial advance occurred as early as ~40 ka (MIS 3) both west and east of the Andean divide arguing for wetter conditions before the gLGM. This agrees with records of Laguna Tagua Tagua, Central Chile documenting increased winter precipitation between ~40-33 ka (Valero-Garcés *et al*., 2005). Riquelme *et al*. (2011) reported radiocarbon ages from the Turbio Valley, Chile (30°S), documenting an extensive glaciation between 37-27 cal. ka BP. Piedmont glaciers in the Chilean Lake District (~40°S, Lowell *et al*., 1995; Denton *et al*., 1999) and in the Andes of Mendoza (33°S, Espizua, 2004, and 32°S, Moreiras *et al*., 2016), reached maxima already at ~40-35 ka as well. We argue that in the semi-arid Central Andes glacial advances at ~40 ka reflect increased winter precipitation attributed to a stronger influence of the Southern Westerlies and more frequent cut offs. Enhanced Southern Westerlies and a stronger Antarctic circumpolar current are, for example, reflected by cooler SST in the SE Pacific (Kaiser *et al*., 2005, 2008). An increased influence of the Southern Westerlies on the hydrological conditions in regions as far as 26°S has also been reported from the Raraku Lake on Easter Island (SE Pacific, 27°S, Sáez *et al*., 2009). There, higher lake levels dominated sedimentation between 34 and 28 cal. ka BP. Additionally, MIS 3 austral winter insolation at 30°S was maximal (Berger

and Loutre, 1991), favouring more humid tropical air in the upper troposphere over the arid Andes. The interaction between cold cut offs coming from the Pacific and warmer, humid air over the continent could thus have generated more snowfall even east of the Andean divide. During austral summer, on the other hand, insolation was minimal and may have favoured cooler summer temperatures and reduced ablation.

The southern and northern Central Andes also document glacial advances in phase with gLGM. Glaciers advanced between ~26-20 ka contemporaneous with lake level highstands recorded in the Uyuni (Baker *et al*., 2001) and Poopo Basin (paleolake Sajsi 24-20.5 ka, Placzek *et al*., 2006, 2011) in response to increased precipitation by an intensified SASM. Humid conditions were also reported for this period off shore Chile, 33°S (Lamy, 1999), in Laguna Tagua Tagua (Chile, 34°30´S, Valero Garcés *et al*., 2005) and in eolian sequences in Argentina (34°S, Tripaldi and Forman, 2016). Maximum austral summer insolation at 30°S (Berger and Loutre, 1991) favoured a southward position of the ITCZ and was conducive for an intensification of the SASM and the upper tropospheric easterlies, so that a combination of globally lower temperatures and insolation minima and more humid conditions seem to have been responsible for glacial advances during the gLGM between 22° and 39°S. Enhanced precipitation during this period, however, has also been explained by a northward shift of the Southern Westerlies, which likely still provided additional precipitation for the gLGM advance in the arid Central Andes (Lamy *et al*., 1999; Kaiser *et al*., 2005; Maldonado *et al*., 2005; Valero-Garcés *et al*., 2005; Kaiser *et al*., 2008), so that the Southern Central Andes likely received precipitation over the whole year during the gLGM. Furthermore, glacial advances attributed to lower temperatures and increased monsoonal precipitation in phase with the gLGM have also been reported north of the Arid Diagonal (May *et al*., 2011; Smith *et al*., 2011; Farber *et al*., 2005).

Deglaciation started along the whole transect at ~18 ka, synchronous with the global atmospheric CO_2 rise and thus increasing temperatures (Shakun *et al*., 2015). Advances are also documented during the late-glacial (here referred to as the period between 18-12 ka) at ~16 ka in the El Encierro valley, the Sierra de Quilmes and Tres Lagunas (29°-22°S) coinciding with a massive lake transgression phase recorded on the Altiplano (Placzek *et al*., 2011) and increased discharge of Río Lluta in northern Chile (Veit *et al*., 2016), implying an increase in precipitation during this time. Further south in the Rucachoroi valley (39°S) a late-glacial glacier is still preserved at ~15 ka. More age control is necessary in order to definitely explain this glacial advance, since topography and the northward exposure of the hill slope might have played a pivotal role. Extensive glacial advances during the late-glacial occurred also further north (~15 and 22°S) in the eastern Cordillera of Argentina and Bolivia. Glaciers advanced before ~14 ka and ~12 ka (Clapperton *et al*., 1997; Clayton and Clapperton, 1997; Zreda *et al*., 2001; Blard *et al*., 2009; Zech R. *et al*., 2007, 2008, 2009; Zech J. *et al*. 2009; May *et al*., 2011) in phase with the Tauca (18.1-14.1 ka) and Coipasa (12.8-11.4 ka) lake transgression phases on the Altiplano, respectively (Clapperton *et al*., 1997; Clayton and Clapperton, 1997; Placzek *et al*., 2006, 2011). These two major lake expansions are part of the Central Andean Pluvial Event (CAPE, 18-8 ka) (Latorre *et al*., 2006; Quade *et al*., 2008), a regional wet phase that impacted regions between 10-26°S. We explain the late-glacial advances recorded in the semi-arid Central Andes by enhanced humidity due to a southward shift of the ITCZ in response to northern hemispheric cooling

during Heinrich I (Heinrich, 1988, Hemming, 2004) and lower temperatures in the eastern equatorial Pacific (Kienast *et al*., 2006; Bova *et al*., 2015) favoring La Niña like conditions bringing more moisture southward. Although south of 30°S the control of the SASM and La Niña-like conditions on late-glacial advances have not been revealed so far, glacial deposits of this age in the Rucachoroi valley could tentatively indicate an influence as far south as 39°S.

6. Conclusions

In the arid Central Andes glaciers are very sensitive to changes in the precipitation regime. Our study shows that glaciations in this region were controlled by latitudinal shifts and intensity changes of the moisture sources, i.e. the tropical circulation system (SASM and ENSO) and the Southern Westerlies.

The oldest dated glaciations in the El Encierro valley probably correspond to global MIS 8 and 6. Glaciations at the southernmost (Rucachoroi valley and Bariloche) and northernmost (Tres Lagunas) sites studied in this work are in phase with the Ouki wet phase on the Altiplano. We argue that these old glaciations may also be moisture driven.

The maximum ice extent for the most extensive glacial advance predating the gLGM maximum during MIS 3 is present in the mid (26° - 30°S) and southern Central Andes (35°-41°S), probably in response to an increased influence of the northward shifted and intensified Southern Westerlies and higher cut off frequency that interacted with the humid air over the continent generating large cloud cluster and increasing austral winter precipitation. This advance highlights the importance of the Southern Westerlies for glacial advances as far north as 26°S.

Glaciers advanced again in phase with the gLGM at ~26-20 ka. This time, however, due to lower temperatures and sufficient humidity provided over the whole year by both the Southern Westerlies and the SASM. The gLGM advance coincides with similar advances further north in NW Argentina, Bolivia and Peru, and with the Sajsi (24.5-20 ka) lake transgression phase on the Altiplano. A global rise in CO_2 and subsequent increase in global temperatures lead to deglaciation across the whole arid Central Andes, starting at ~18 ka. La Niña-like conditions and the intensified SASM enhanced the upper tropospheric easterlies and provided sufficient moisture for the massive late-glacial advance recorded in the northernmost part of the transect presented here and also tentatively as south as 39°S.

7. Acknowledgements

We thank Anina Schmidhauser and Christoph Bächtiger for helping with fieldwork and laboratory analyses. J.Z. thanks Thomas Nägler and Igor Villa for providing laboratory facilities at the Institute of Geology, University of Bern. For helpful discussions and local logistic support we thank Grupo Yavi de Investigaciones Científicas, especially Liliana Lupo and Julio Kuhlemeier. This work was financially supported by the Swiss National Fund (Project 200020-113461/1). The authors thank Jesús Ruiz Fernández and an anonymous reviewer for the helpful feedback.

References

Ammann C., Jenny, B., Kammer, K., Messerli, B. 2001. Late Quaternary Glacier response to humidity changes in the arid Andes of Chile (18-29ºS). *Palaeogeography, Palaeoclimatology, Palaeoecology* 172, 313-326. http://doi.org/10.1016/S0031-0182(01)00306-6.

Baker, P.A., Rigsby, C.A., Seltzer, G.O., Fritz, S.C., Lowenstein, T.K., Bacher, N.P., Veliz, C. 2001. Tropical climate changes at millenial and orbital timescales on the Bolivian Altiplano. *Nature* 409, 698-701. http://doi.org/10.1038/35055524.

Berger, A., Loutre, M.F. 1991. Insolation values for the climate of the last 10 million years. *Quaternary Sciences Reviews* 10 (4), 297-317. http://doi.org/10.1016/0277-3791(91)90033-Q.

Bianchi, A.R., Yáñez, C.E. 1992. *Las Precipitaciones en el Noroeste Argentino*. Instituto Nacional de Tecnología Agropecuaria (INTA), Argentina.

Blard, P.-H., Lave, J., Farley, K.A., Fornari, M., Jimenez, N., Ramirez,V. 2009. Late local glacial maximum in the Central Altiplano triggered by cold and locally-wet conditions during the paleolake Tauca episode (17-15 ka, Heinrich 1). *Quaternary Science Reviews* 27-28, 3414-3427. http://doi.org/10.1016/j.quascirev.2009.09.25.

Bova, S.C., Herbert, T., Rosenthal, Y., Kalansky, J., Altabet, M., Chazen, C., Mojarro, A., Zech, J. 2015. Links between eastern equatorial Pacific stratification and atmospheric CO_2 rise during the last deglaciation. *Paleoceanography* 30, 11, 1407-1424. http://doi.org/10.1002/2015PA002816.

Briner, J.P., Kaufman, D.S., Manley, W.F., Finkel, R.C., Caffee, M.W. 2005. Cosmogenic exposure dating of late Pleistocene moraine stabilization in Alaska. *Geological Society of America Bulletin* 117, 1108-1120.

Chmeleff, J., von Blanckenburg, F., Kossert, K., Jakob, D. 2010. Determination of the ^{10}Be half-life by multicollector ICP-MS and liquid scintillation counting. *Nuclear Instruments and Methods in Physics Research Section B: Beam Interactions with Materials and Atoms* 268 (2), 192-199. http://doi.org/10.1016/j.nimb.2009.09.012.

Clapperton, C.M., Clayton, J.D., Benn, D.I., Marden, C.J., Argollo, J. 1997. Late Quaternary glacier advances and paleolake highstands in the Bolivian Altiplano. *Quaternary International* 38-39, 49-59. http://doi.org/10.1016/S1040-6182(96)00020-1.

Clark, P.U., Dyke, A.S., Shakun, J.D., Carlson, A.E., Clark, J., Wohlfarth, B., Mitrovica, J.X., Hostetler, S.W., McCabe, A.M. 2009. The Last Glacial Maximum. *Science* 325, 710.

Clayton, J.D., Clapperton, C.M. 1997. Broad synchrony of a Late-Glacial glacier advance and the highstand of Palaeolake Tauca in the Bolivian Altiplano. *Journal of Quaternary Science* 12, 169-182.

Denton, G.H., Lowell, T.V., Heusser, C.J., Schlüchter, C., Andersen, B.G., Heusser, L.E., Moreno, P.I., Marchant, D.R. 1999. Geomorphology, stratigraphy, and radiocarbon chronology of Llanquihue drift in the area of the southern Lake District, Seno Reloncavi, and Isla Grande de Chiloe, Chile. *Geografiska Annaler* 81A, 167-229. http://doi.org/10.1111/1468-0459.00057.

Espizua, L.E. 2004. Pleistocene glaciations in the Mendoza Andes, Argentina. In: J. Ehlers, P.L. Gibbard (Eds.), *Quaternary Glaciations - Extent and Chronology. Part III: South America, Asia, Africa, Australasia, Antarctica*. Cambridge, Elsevier.

Farber, D.L., Hancock, G.S., Finkel, R.C., Rodbell, D.T. 2005. The age and extent of tropical alpine glaciation in the Cordillera Blanca, Peru. *Journal of Quaternary Science* 20, 759-776. http://doi.org/10.1002/jqs.994.

Garreaud, R., Aceituno, P. 2001. Interannual Rainfall Variability over the South American Altiplano. *Journal of Climate* 14 (12), 2779-2789.

Garreaud, R., Aceituno, P. 2007. Atmospheric circulation and climatic variability. In: T.T. Veblen, K.R. Young, A.R. Orme (Eds.) *The physical geography of South America*. Oxford University Press, Oxford.

Garreaud, R., Vuille, M., Clement, A.C. 2003. The climate of the Altiplano: observed current conditions and mechanisms of past changes. *Palaeogeography, Palaeoclimatology, Palaeoecology* 194 1-3, 5-22. http://doi.org/10.1016/S0031-0182(03)00269-4.

Garreaud, R.D., Vuille, M., Compagnucci, R., Marengo, J. 2009. Present-day South American climate. *Palaeogeography, Palaeoclimatology, Palaeoecology* 281 (3-4), 180-195. http://doi.org/10.1016/j.palaeo.2007.10.032.

Haselton, K., Hilley, G, Strecker, M.R. 2002. Average Pleistocene Climatic Patterns in the Southern Central Andes: Controls on Mountain Glaciation and Paleoclimate Implications. *The Journal of Geology* 110 (2), 211-226. http://doi.org/10.1086/338414.

Heinrich, H. 1988. Origin and consequences of cyclic ice rafting in the Northeast Atlantic Ocean during the past 130,000 years. *Quaternary Research* 29 (2), 142-152. http://doi.org/10.1016/0033-5894(88)90057-9.

Hemming, S.R. 2004. Heinrich Events: Massive late Pleistocene detritus layers of the North Atlantic and their global climate imprint. *Reviews of Geophysics* 42, RG1005. http://doi.org/10.1029/2003RG000128.

Heyman, J., Stroeven, A.P., Harbor, J.M., Caffee, M.W. 2011. Too young or too old: Evaluating cosmogenic exposure dating based on an analysis of compiled boulder exposure ages. *Earth and Planetary Science Letters* 302 (1-2), 71-80. http://doi.org/10.1016/j.epsl.2010.11.040.

Kaiser, J., Lamy, F., Hebbeln, D. 2005. A 70-kyr sea surface temperature record off southern Chile (Ocean Drilling Program Site 1233). *Paleoceanography* 20 (4), PA4009. http://doi.org/10.1029/2005PA001146.

Kaiser, J., Schefuß, E., Lamy, F., Mohtadi, M., Hebbeln, D. 2008. Glacial to Holocene changes in sea surface temperature and coastal vegetation in north central Chile: high versus low latitude forcing. *Quaternary Science Reviews* 27, 2064-2075. http://doi.org/10.1016/j.quascirev.2008.08.025.

Kienast, M., Kienast, S.S., Calvert, S.E., Eglington, T.I., Mollenhauer, G., Francois, R., Mix, A.C. 2006. Eastern Pacific cooling and Atlantic overturning circulation during the last deglaciation. *Nature* 443, 846-849. http://doi.org/10.1038/nature05222.

Kubik, P.W., Christl, M. 2010. ^{10}Be and ^{26}Al measurements at the Zurich 6 MV Tandem AMS facility. *Nuclear Instruments and Methods in Physics Research B Beam Interactions with Materials and Atoms* 268 (7-8), 880-883. http://doi.org/10.1016/j.nimb.2009.10.054.

Korschinek, G., Bergmaier, A., Faestermann, T., Gerstmann, U.C., Knie, K., Rugel, G., Wallner, A., Dillmann, I., Dollinger, G., von Gostomski, C.L., Kossert, K., Maiti, M., Poutivtsev, M., Remmert, A. 2010. A new value for the half-life of ^{10}Be by Heavy-Ion Elastic Recoil Detection and liquid scintillation counting. *Nuclear Instruments and Methods in Physics Research Section B: Beam Interactions with Materials and Atoms* 268 (2), 187-191. http://doi.org/10.1016/j.nimb.2009.09.020.

Kull, C., Grosjean, M. Veit, H. 2002. Modeling Modern and Late Pleistocene Glacio-Climatological Conditions in the North Chilean Andes (29-30°). *Climatic Change* 52, 359-381. http://doi.org/10.1023/A:1013746917257.

Kull, C., Imhof, S., Grosjean, M., Zech, R., and Veit, H. 2008. Late Pleistocene glaciation in the Central Andes: Temperature versus humidity control - A case study from the eastern Bolivian Andes (17°S) and regional synthesis. *Global and Planetary Change* 60, 148-164. http://doi.org/10.1016/j.gloplacha.2007.03.011

Lamy, F., Hebbeln, D., Wefer, G. 1999. High-Resolution Marine Record of Climatic Change in Mid-latitude Chile during the Last 28,000 Years Based on Terrigenous Sediment Parameters. *Quaternary Research* 51 (1), 83-93.

Latorre, C., Betancourt, J.L., Arroyo, M.T.K. 2006. Late Quaternary vegetation and climate history of a perennial river canyon in the Rio Salado basin (22°S) of Northern Chile. *Quaternary Research* 65 (3), 450-466. http://doi.org/10.1016/j.yqures.2006.02.002.

Lifton, N., Sato, T., Dunai, T.J. 2014. Scaling in situ cosmogenic nuclide production rates using analytical approximations to atmospheric cosmic-ray fluxes. *Earth and Planetary Science Letters* 386, 149-160. http://doi.org/10.1016/j.epsl.2013.10.052.

Lowell, T.V., Heusser, C.J., Andersen, B.G., Moreno, P.I., Hauser, A., Heusser, L.E., Schlüchter, C., Marchant, D.R., Denton, G.H. 1995. Interhemispheric correlations of Late Pleistocene glacial events. *Science* 269, 1541-1549. http://doi.org/10.1126/science.269.5230.1541.

Maldonado, A., Betancourt, J.L., Latorre, C., Villagran, C. 2005. Pollen analyses from a 50,000-yr rodent midden series in the southern Atacama Desert (25° 30' S). *Journal of Quaternary Science* 20 (5), 493-507. http://doi.org/10.1002/jqs.936.

Marrero, S.M., Phillips, F.M., Borchers, B., Lifton, N., Aumer, R., Balco, G. 2016. Cosmogenic nuclide systematics and the CRONUScalc program. *Quaternary Geochronology* 31, 160-187.

May, J.-H., Zech, J., Zech, R., Preusser, F., Argollo, J., Kubik, P., Veit, H. 2011. Reconstruction of a complex late Quaternary glacial landscape in the Cordillera de Cochabamba (Bolivia) based on a morphostratigraphic and multiple dating approach. *Quarternary Research* 76, 106-118. http://doi.org/10.1016/j.yqres.2011.05.003.

Moreiras, S.M., Páez, M.S., Lauro, C., Jeanneret, P. 2016. First cosmogenic ages for glacial deposits from the Plata range (33°S): New inferences for Quaternary landscape evolution in the Central Andes. *Quaternary International* 438, 50-64, http://dx.doi.org/10.1016/j.quaint.2016.08.041.

Peltier, W.R., Fairbanks, R.G. 2006. Global glacial ice volume and Last Glacial Maximum duration from an extended Barbados sea level record. *Quaternary Science Reviews* 25, 3322-3337. http://doi.org/10.1016/j.quascirev.2006.04.010.

Phillips, F.M., Argento, D.C., Balco, G., Caffee, M.W., Clem, J., Dunai, T.J., Finkel, R., Goehring, B., Gosse, J.C., Hudson, A.M., Jull, A.J.T., Kelly, M.A., Kurz, M., Lal, D., Lifton, N., Marrero, S.M., Nishiizumi, K., Reedy, R.C., Schaefer, J., Stone, J.O.H., Swanson, T., and Zreda, M.G. 2016. The CRONUS-Earth Project: A Synthesis, *Quaternary Geochronology* 31, 119-154. http://doi.org/10.1016/j.quageo.2015.09.006.

Placzek, C., Quade, J., Patchett, J.P. 2006. Geochronology and stratigraphy of late Pleistocene lakes cycles on the southern Bolivian Altiplano: Implications for causes of tropical climate change. *Geological Society of America Bulletin* 118, 515-532.

Placzek, C., Quade, J., Patchett, P.J. 2011. Isotopic tracers of paleohydrologic change in large lakes of the Bolivian Altiplano. *Quaternary Research* 75 (1), 231-244. http://doi.org/10.1016/j.yqres.2010.08.004.

Putkonen, J. Swanson, T. 2003. Accuracy of cosmogenic ages for moraines. *Quarternary Research* 59, 255-261. http://doi.org/10.1016/S0033-5894(03)00006-1.

Quade, J., Rech, J.A., Betancourt, J.L., Latorre, C., Quade, B., Rylander, K.A., Fisher, T. 2008. Paleowetlands and regional climate change in the central Atacama Desert, northern Chile. *Quaternary Research* 69 (3), 343-360. http://doi.org/10.1016/j.yqres.2008.01.003.

Riquelme, R., Rojas, C., Aguilar, G., Flores, P. 2011. Late Pleistocene-early Holocene paraglacial and fluvial sediment history in the Turbio valley, semiarid Chilean Andes. *Quaternary Research* 75 (1), 166-175. http://doi.org/10.1016/j.yqres.2010.10.001.

Rodbell, D.T., Smith, J.A., Mark, B.G. 2009. Glaciation in the Andes during the Lateglacial and Holocene. *Quaternary Science Reviews* 28, 2165-2212. http://doi.org/10.1016/j.quascirev.2009.03.012.

Sáez, A., Valero-Garcés, B.L., Giralt, S., Moreno, A., Bao, R., Pueyo, J.J., Hernández, A., Casas, D. 2009. Glacial to Holocene climate changes in the SE Pacific. The Raraku Lake sedimentary record (Easter Island, 27°S). *Quaternary Science Reviews* 28 (25-26), 2743-2759. http://doi.org/10.1016/j.quascirev.2009.06.018.

Shakun, J.D., Clark, P.U., He, F., Lifton, N.A., Liu, Z., Otto-Bliesner, B.L. 2015. Regional and global forcing of glacier retreat during the last deglaciation. *Nature Communications* 6, 8059. http://doi.org/10.1038/ncomms9059.

Smith, C.A., Lowell, T.V., Owen, L.A., Caffee, M.W. 2011. Late Quaternary glacial chronology on Nevado Illimani, Bolivia, and the implications for paleoclimatic reconstructions across the Andes. *Quaternary Research* 75 (1), 1-10. http://doi.org/10.1016/j.yqres.2010.07.001.

Terrizzano, C., Zech, R., García Morabito, E., Haghipour, N., Christl, M., Likermann, J., Tobal, J., Yamin, M. 2016. Surface exposure dating of moraines and alluvial fans in the Southern Central Andes. *Geophysical Research Abstracts*, 18, EGU2016-15358.

Tripaldi, A., Forman, S.L. 2016. Eolian depositional phases during the past 50 ka and inferred climate variability for the Pampean Sand Sea, western Pampas, Argentina. *Quaternary Science Reviews* 139, 77-93. http://doi.org/10.1016/j.quascirev.2016.03.007.

Valero-Garcés, B.L., Jenny, B., Rondanelli, M., Delgado-Huertas, A., Burns, S.J., Veit, H., Moreno, A. 2005. Palaeohydrology of Laguna de Tagua Tagua (34° 30' S) and moisture fluctuations in Central Chile for the last 46 000 yr. *Journal of Quaternary Science* 20 (7-8), 625-641. http://doi.org/10.1002/jqs.988.

Veit, H., May, J-H., Madella, A., Delunel, R., Schlunegger, F., Szidat, S., Capriles, J.M. 2016. Palaeo-geoecological significance of Pleistocene trees in the Lluta Valley, Atacama Desert. *Journal of Quaternary Science* 31 (3), 203-213. http://doi.org/10.1002/jqs.2857.

Vuille, M. Ammann, C. 1997. Regional snowfall patterns in the high, arid Andes (South America). *Climatic Change* 36, 413-423. http://doi.org/10.1023/A:1005330802974.

Vuille, M., Bradley, R.S., Keimig, F. 2000. Interannual climate variability in the Central Andes and its relation to tropical Pacific and Atlantic forcing. *Journal of Geophysical Research* 105 D10, 12447-12460. http://doi.org/10.1029/2000JD900134.

Vuille, M., Keimig, F. 2004. Interannual variability of summertime convective cloudiness and precipitation in the Central Andes derived from ISCCP-B3 Data. *Journal of Climate* 17, 3334-3348. http://doi.org/10.1175/1520-0442(2004)017<3334:IVOSCC>2.0.CO;2.

Wäger, P. 2009. *Glacier-climate modelling in Las Leñas, Central Andes of Argentina*. Master Thesis, Faculty of Sciences, University of Bern, 135 pp.

Zech, J., Zech, R., Kubik, P.W., Veit, H. 2009. Glacier and climate reconstruction at Tres Lagunas, NW Argentina, based on 10Be surface exposure dating and lake sediment analyses. *Palaeogeography, Palaeoclimatology, Palaeoecology* 284, 180-190. http://doi.org/10.1016/j.palaeo.2009.09.23

Zech, R., Glaser, B., Sosin, P., Kubik, P.W., Zech, W. 2005. Evidence for long-lasting landform surface instability on hummocky moraines in the Pamir Mountains (Tajikistan) from 10Be surface exposure dating. *Earth and Planetary Science Letters* 237 (3-4), 453-461. http://doi.org/10.1016/j.epsl.2005.06.31.

Zech, R., Kull, C., Kubik, P.W., Veit, H. 2007. LGM and Late Glacial glacier advances in the Cordillera Real and Cochabamba (Bolivia) deduced from 10Be surface exposure dating. *Climate of the Past* 3, 623-635.

Zech, R., May, J.-H., Kull, C., Ilgner, J., Kubik, P.W., Veit, H. 2008. Timing of the late Quaternary glaciation in the Andes from ~15 to 40° S. *Journal of Quaternary Science* 23, 635-647. http://doi.org/10.1002/jqs.1200.

Zech, R., Smith, J., Kaplan, M. 2009. Chronologies of the LGM and its Termination in the Andes based on Surface Exposure Dating. In: F. Vimeux, F. Sylvestre, M. Khodri (Eds.), *Past climate variability in South America and surrounding regions. From the Last Glacial Maximum to the Holocene*. Springer, pp. 61-87.

Zhou, J., Lau, K.M. 1998. Does a monsoon climate exist over South America? *Journal of Climate* 11, 1020-1040.

Zreda, M., Clapperton, C., Argollo, J., Shanahan, T. 2001. Evidence for contemporary lakes and glaciers in the southern Altiplano during late glacial time. *Fifth Iberian Quaternary Meeting* (extended abstract), Lisboa, Portugal.